EXPERIMENTAL INVESTIGATION OF ROTOR VORTEX WAKES IN DESCENT

James Stack
University of California Berkeley

Keywords: *helix rotor visualization vortex wake*

Abstract

An experimental study is performed on a three-bladed rotor model in two water tanks. The blade pitch, rotational velocity, descent angle, and descent speed are all varied in order to simulate a wide range of rotorcraft operating states, with the focus being on descent cases where the rotor is operating in or near vortex ring state – an area in which there is currently very little available data. Flow visualization is done by injecting air bubbles and fluorescent dye tangentially from the blade tips to mark the vortex core, showing the development of both short-wave ("sinuous") and long-wave ("leapfrogging") instabilities on the helical vortices in the wake. Strain gages are used to record transient loads, allowing a correlation between the rotor thrust performance and the development of the vortex wake. Reynolds numbers are of order 10^5 *and test runs are performed for extended periods – up to 500 rotor revolutions – demonstrating the repeatability of the patterns of thrust variation. The data indicate that as the instabilities develop, adjacent vortices merge and form thick vortex rings, particularly during descent. Periodic shedding of these rings from the wake associated with vortex ring state is observed, resulting in peak-to-peak thrust fluctuations of up to 95% of the mean and occurring at regular intervals of 20–50 rotor revolutions, depending on flow parameters.*

1 General Introduction

An accurate understanding of the physics of helical vortex wakes has long been regarded as one of the most difficult problems in fluid dynamics. Even before the days of modern production helicopter flight, the issue of the nature and stability of ring vortices and helical vortices had been analyzed extensively. Levy and Forsdyke [1] performed a stability analysis on a single helical vortex in 1928, and more recently, Landgrebe [2] and Widnall [3] have added to and corrected this study. Gupta and Loewy [4] have performed a similar stability analysis on multiple interdigitated helical vortices.

Despite the focus that modern helicopter flight has brought to the problem in the last hundred years, and despite the power of modern computers and experimental tools, a true grasp of the physics of helical vortices has remained elusive. While somewhat reasonable approximations of their behavior can be made under highly simplified scenarios, there is much progress still to be made on the problem of *real* helical vortices. In fact, not even the simplest case of a stationary (hovering) rotor generating a steady, vertical, helical wake can be computationally modeled with much accuracy at distances greater than one or two diameters downstream of the rotor.

The problem for aerodynamicists is that the flight regimes that are of greatest interest to the rotorcraft community are precisely the ones that are most difficult to analyze.

When a helicopter is descending rapidly, the very thing that makes the wake solution so challenging – the intense interaction between the rotor and its vortex wake – causes large, unsteady dynamic loads on the blades. Under certain circumstances (when the rotor descent velocity approximately matches the wake velocity), the aircraft can encounter a condition known as vortex ring state (VRS), where the tip vortices merge together, forming a thick vortex ring that remains near the rotor plane, disrupting the inflow and causing a dramatic reduction in lift. This unstable ring typically undergoes an almost periodic shedding and reformation pattern that results in large fluctuations in thrust that make the aircraft quite difficult to control. As retired test pilot Mott F. Stanchfield says, "In my opinion, a mature VRS is the most hazardous condition that exists in the realm of helicopter aeronautics" [5].

Although the aerodynamics of rotors in descending flight – and in VRS in particular – has been the subject of research for many years (see [6, 7, 8, 9, 10]), that work has largely focused on measurements of the rotor airloads with very little flow field visualization, and even less simultaneous measurement of airloads and flow fields. This is likely due to the relative "disorder" of such flows and the difficulties associated with facility/model sizing, turbulent diffusion, and injection of flow markers. The present study is aimed at addressing these difficulties and providing a relatively complete description of the wake of the descending rotor and its effect on rotor loading.

Flow visualization and thrust measurement results are presented from experiments performed on a model rotor in a wide range of operating states – from hover to forward flight to rapid descent – with the focus being on the VRS regime. Experiments were performed in a 60 m long water tow tank, which allowed for extended run times that were more than sufficient for the study of long-period unsteady flows such as those encountered in descending flight. The rotor's performance is quantified by measurements of its thrust, and this information is correlated with simultaneous flow visualization images.

The time-history characteristics of the rotor's thrust are examined for a broad range of descent speed, descent angle, and collective angle combinations. By testing the rotor in a wide variety of configurations, the rotor's performance can be fully characterized, and the descent conditions in which VRS behavior is observed can be clearly identified. The thrust time-histories of these cases are then compared in order to determine how the descent configuration affects the amplitude, frequency, and overall "orderliness" of the observed thrust fluctuations. For these particular cases, the flow visualization images of the experiment provide clues as to the nature of the vortex wake formation and shedding phenomenon that makes VRS such a dangerous flight regime.

2 Experimental Setup

2.1 Rotor Model

Experiments were performed with a three-bladed 25.4 cm diameter rotor model featuring manually adjustable blade pitch. The blades (Fig. 1), which were 9.5 cm long, were molded from carbon fiber plastic. The blades were untapered, with a 1.9 cm chord, and had a twist of about 5° (compared with twists of 35–40° for typical tilt-rotor aircraft). The low blade twist was chosen in order to maintain a clean flow over the blades and also to minimize rotor separation. The blade airfoils were modified ARAD-10 at the tip and modified ARAD-13 at the root. Each blade had a 0.36 mm ID stainless steel tube embedded along its span, allowing dye or air to be injected into the flow from the tip to mark the vortex cores. The airfoil modifications included a chordwise-linear thickness increase which thickened the trailing edge and provided more room for the dye/air tubes. In addition, the aft camber of the root airfoil was increased.

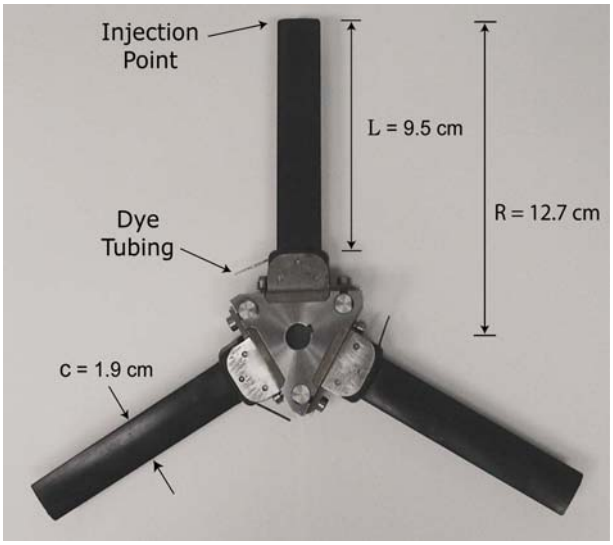

Fig. 1 Model 3-bladed rotor. Diameter is 25.4 cm. Dye and air enter the tubes at the root, flow through the blades to the tips, and enter the flow tangentially.

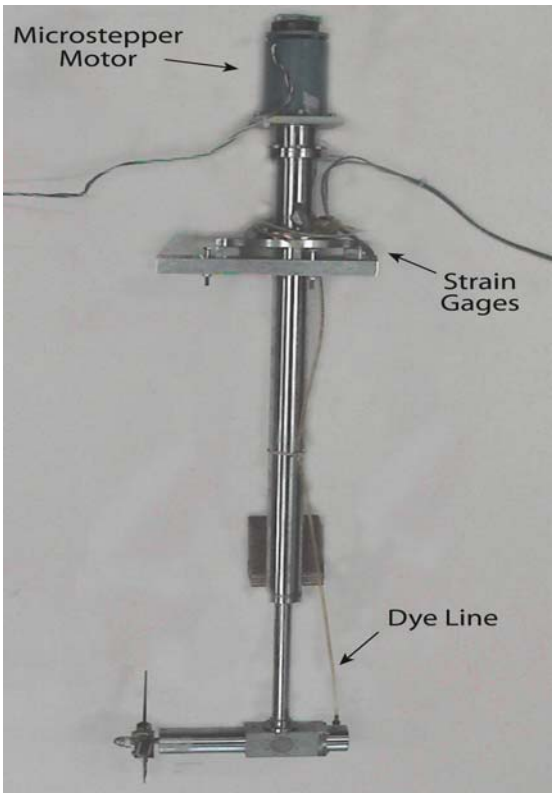

Fig. 2 Entire model assembly, with locations of strain gages and dye tubing. Flow would be from left to right in descent.

The rotor was driven by a digitally-controlled microstepper motor (25,000 pulses per revolution), allowing for precise control of both the rotor's position and velocity. The motor was mounted atop an 89 cm vertical shaft and drove a 23 cm horizontal shaft onto which the rotor was fixed (Fig. 2). The vertical shaft lay downstream of the rotor during descent testing, so as to avoid interfering with the rotor's inflow. Just beneath the motor was a 2.5 cm thick rectangular mounting plate which supported the model assembly and also measured rotor thrust, using a pair of flexures instrumented with 120 ohm strain gage bridges. The thrust readings were fed to the computer controlling the experiment. The gages were calibrated to produce thrust readings in units of force, and also to correct for the drag force on the model as it was pulled through the water. Data are band-pass filtered during post-processing to eliminate high-frequency electrical and vibrational noise while retaining the main features of the signal.

To visualize the rotor's wake, air bubbles and sodium fluorescent dye were released from the blade tips in a direction tangential to the blade path. The dye and air were supplied to the dye reservoir at the base of the vertical shaft through thin, flexible plastic tubing (Fig. 2). The dye reservoir was directly connected to the rotor dye tubes through the horizontal drive shaft. The pressure deficit at the blade tips drew some fluid from the supply tube into the wake, but in order to achieve clear visualization of the flow it was necessary to supply external pressure.

2.2 Stationary Tank

Initial testing was performed in a 1.22 × 2.44 × 1.68 m deep stationary water tank at the University of California Berkeley. With the model fixed in place atop the tank, these tests simulated a hovering helicopter's flow field. A 10-W Argon ion laser provided both planar and volumetric illumination. For the two-dimensional lighting tests, a vertical light sheet was aligned with the axis of the rotor. In

all cases, a digital video camera recorded the flow from the side of the tank, perpendicular to the wake direction and the light sheet. Due to the small size of the tank, test runs were relatively brief (and between-test intervals relatively long) in order to minimize recirculation effects which would lead to an unwanted climb condition.

Generally, air was used as the injection fluid for initial experiments because of its non-contaminating nature. Also, in contrast to the neutrally-buoyant dye, which marked the vortex cores but diffused to areas surrounding the core as well, the majority of the air bubbles initially migrated directly to the low pressure vortex cores. Thus in the near-wake of the rotor, before the vorticity had diffused significantly and attenuated the pressure deficit at the cores, the air bubbles nicely captured the details of the filament structure. However, once the transition to the far-wake region occurred, the buoyancy of the bubbles caused them to rise to the surface quickly, rendering the details of the wake indecipherable for distances greater than about one diameter downstream of the rotor. Later tests used neutrally-buoyant fluorescent dye as the injection fluid, which clearly showed the break-up and diffusion of the wake at greater downstream distances. In general, thrust measurements were not recorded for the stationary tank tests. Rather, these tests were performed primarily for visualization purposes, as the quality of the images was significantly better in the stationary tank than in the towing tank and the structure and evolution of the wake could more clearly be discerned.

2.3 Towing Tank

The characteristics of a descending helicopter were simulated by pulling the model through water in the 60 m long tow tank at the University of California's Richmond Field Station. The 2.4 m wide, 1.5 m deep tank features a large, low-speed carriage running along a set of rails on top of the tank. The carriage speed, which for these tests ranged from 0–50 cm/s, could be controlled manually or by computer.

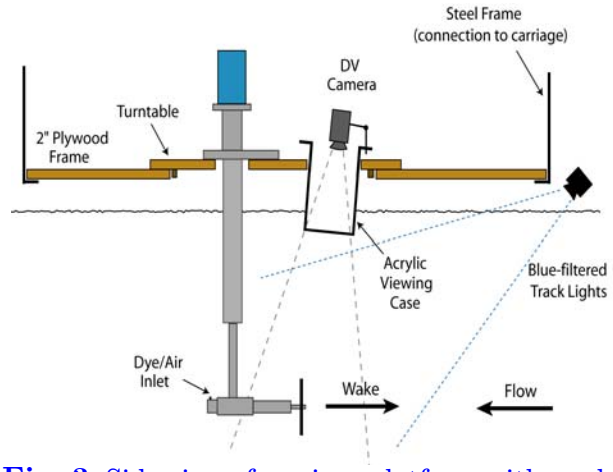

Fig. 3 Side view of carriage platform with model assembly mounted on turntable. Direction of travel is from left to right.

The model assembly (Fig. 2) was mounted on a 1.22 × 1.52 m plywood platform, which was suspended just above the water surface by a steel frame connected to the carriage (Fig. 3). The model could be rotated using a turntable on the plywood platform, enabling the descent angle of the rotor to be varied in 0.5° increments, from 0° (forward flight) to 90° (vertical descent). A set of halogen track lights with blue dichroic filters was mounted onto the front of the carriage to illuminate the flow and highlight the yellow fluorescent dye. Unfiltered white light was used when air was the injection fluid. For visualization, the video camera was mounted on the platform vertically, looking downward at the flow and fixed in position with respect to the rotor.

3 Results

All results presented in this paper, unless stated otherwise, refer to experiments conducted at a rotor rotation rate of Ω=4 rev/s (V_{tip}=319 cm/s). This was taken as a representative case in order to limit the number of experimental variables and also because it produced the best flow visualization results. In addition, since rotor thrust is proportional to the square of the rotation rate, the *non-*

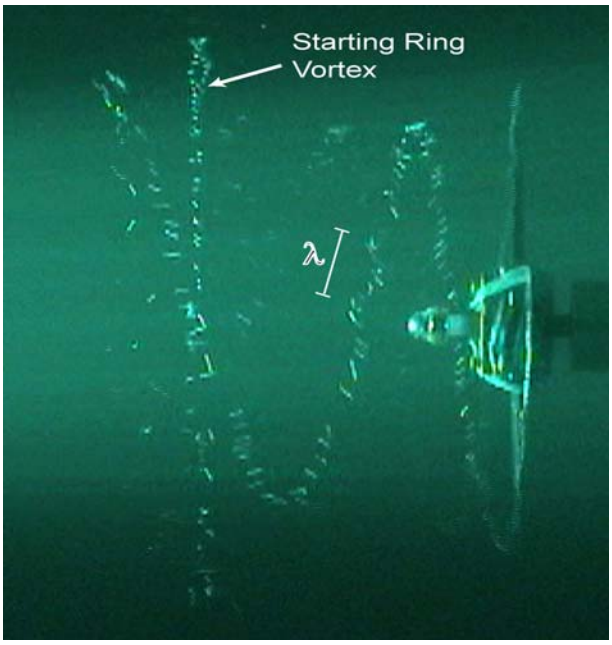

Fig. 4 Three-dimensional flow visualization image of rotor using air injection from tip of one blade. Rotor speed is Ω=3 rev/s. The short-wave sinuous instability of the vortex is just visible.

dimensional thrust coefficient C_T is essentially independent of rotation rate, being a function of the rotor/airfoil geometry and the blade pitch angle only.

3.1 Flow Visualization

Flow visualization testing in the stationary water tank yielded numerous images clearly showing the development of the rotor wake and the instabilities that cause it to break down. In Fig. 4, air bubbles are injected from the tip of only one blade for the sake of clarity. The large starting ring vortex can be seen on the left, expanding and slowing down as the rest of the wake passes through it. In this three-dimensional image, the short-wave "smooth sinuous wave type" instability – which was discussed by Fukumoto and Miyazaki [11] and analyzed theoretically by Widnall [3] and Gupta and Loewy [4] – can clearly be seen along the filament in the near-wake of the rotor. Ortega *et al.* [12] have suggested that this is an elliptic instability of the vortex cores that develops cooperatively on adjacent helix turns, though this observation is unable to be verified here with air being released from only one blade. In this case the wavelength of the instability is approximately 3.75 cm, or 2c.

Figure 5 shows a series of two-dimensional images of the upper half of the rotor plane with dye being injected from all three blade tips. This view of the wake shows cross-sections of the cores of the three tip vortices and illustrates the influence that each vortex filament has on its neighbors. The induced velocities of adjacent turns cause the helices to expand and contract, thus altering their propagation speeds and resulting in the classic "leapfrogging" or "vortex pairing" phenomenon often seen with parallel vortex rings. This effect – which was studied computationally by Jain and Conlisk [13] and experimentally by Ortega *et al.* [12] – can be seen in the pairing of the second and third vortex cores downstream of the rotor in (b) and (c), and quickly leads to the complete merger of all three vortices in (e). The merger of adjacent tip vortices is a general phenomenon of rotors regardless of the number of blades – for example, Ortega *et al.* [12] observed it in the wake of a two-bladed rotor. However, with fewer blades the adjacent helix turns are farther apart and thus the leapfrogging and merging processes take longer to transpire. The location where the three vortices merge – about half a diameter downstream of the rotor – can be taken as the point where the wake loses its helical structure.

3.2 Thrust Measurements

Instantaneous thrust measurements were recorded during the descent experiments in the towing tank. These tests were conducted over a range of towing speeds from 0–50 cm/s, descent angles from α=0–90°, and collective angles from θ=6–18°. Descent runs were typically performed for 100 rotor revolutions, although some were conducted for longer periods in order to verify the trends observed dur-

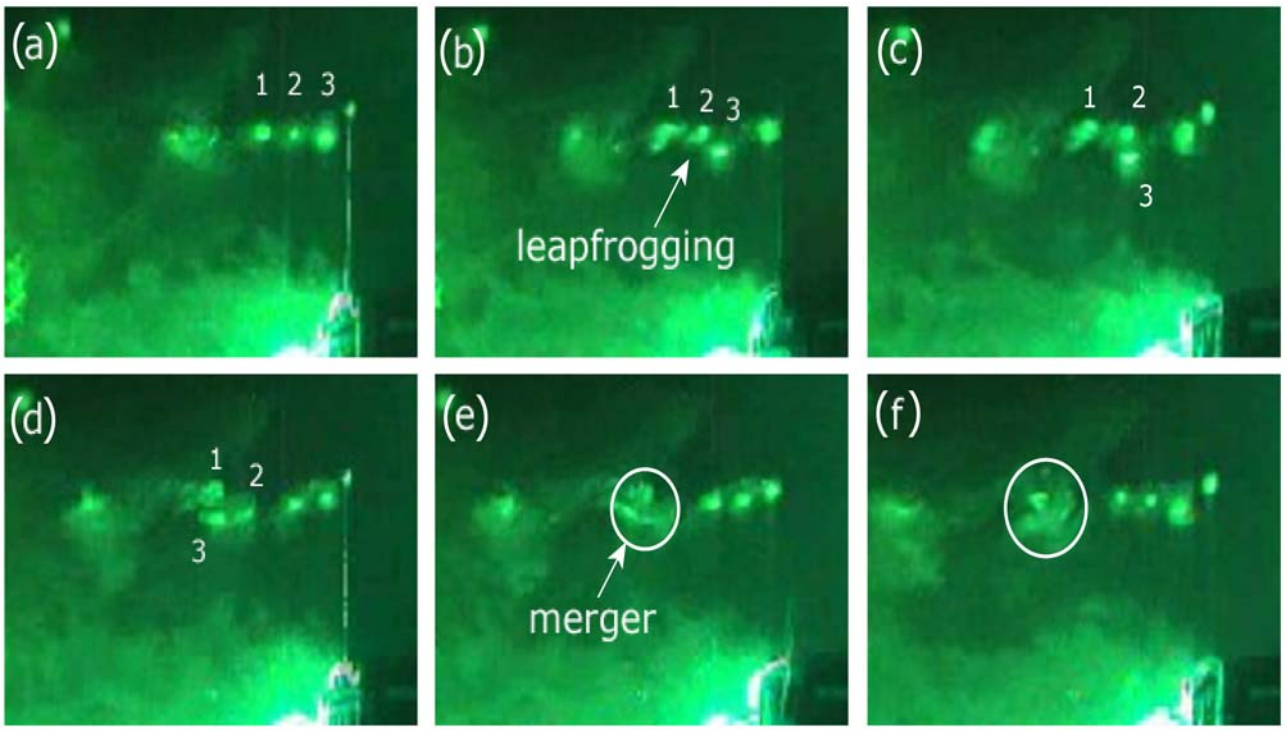

Fig. 5 Two-dimensional flow visualization images of upper half of rotor in hover using fluorescent dye injection from all three blade tips. The "leapfrogging" of one vortex filament over another can be seen in (b) and (c) as the three vortices orbit about each other and finally merge in (e).

ing shorter runs. The data sampling rate was 200 samples per revolution, and the first and last five revolutions of the run were ignored (due to the starting transients from the carriage motion, and also to the width of the filtering window).

For many of the runs, thrust levels remained relatively steady over the duration of the experiment. This was generally the case for hover, slow descent, and very steep or very shallow descent angle runs. Figure 6 shows a thrust coefficient time-history for a hovering rotor. The mean thrust coefficient was 0.0078 and the peak-to-peak fluctuation amplitude was 12% of the mean. Figure 7 shows a thrust coefficient time-history of similar form, but for a rapid descent at a fairly shallow descent angle (α=30°). Note that the mean thrust coefficient, 0.018, is more than two times greater than in the hover case, but the total fluctuation amplitude is still only 12% of the mean.

However, for experiments featuring a combination of moderate descent speed and steep

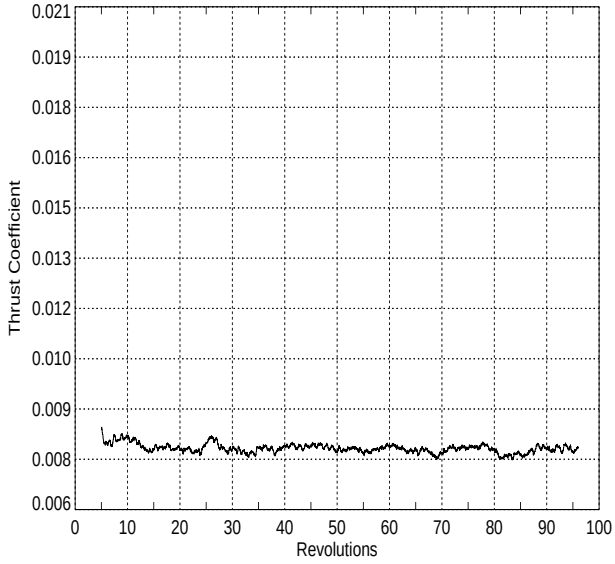

Fig. 6 Thrust time-history for a hover test (μ=0). Mean thrust coefficient is 0.0078 and fluctuation is 12% of the mean.

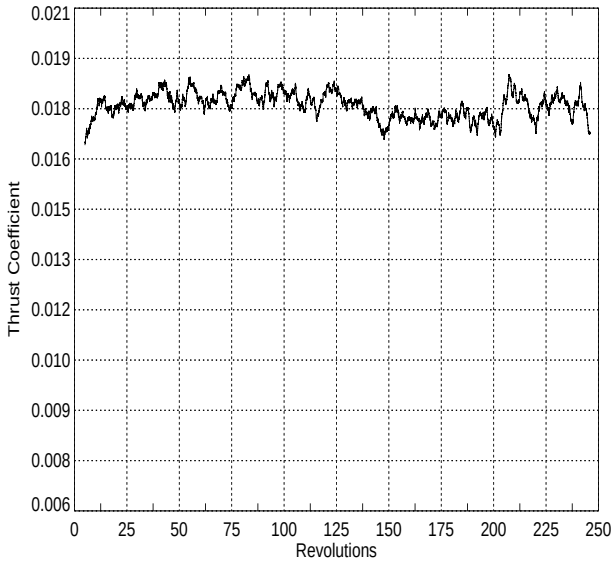

Fig. 7 Thrust time-history for a fast, shallow descent run (μ=0.102). Mean thrust coefficient is 0.0181 and fluctuation is 12% of the mean.

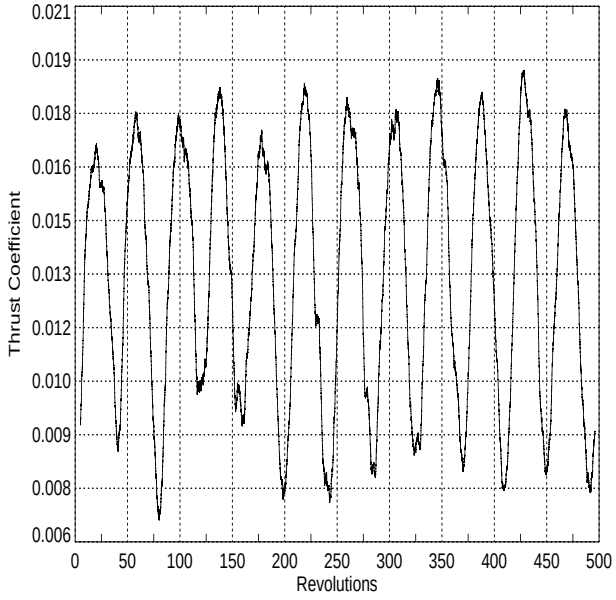

Fig. 8 Thrust time-history for a classic VRS case: α=60°, V=25 cm/s (μ=0.039). Mean thrust coefficient is 0.0135, fluctuation amplitude is 94% of the mean, and fluctuation period is about 43 revolutions.

descent angle, the rotor thrust characteristics were markedly different. In some such cases, the thrust exhibited very large, regular fluctuations. Figures 8–9, for instance, show thrust time-histories typical of this type of behavior.

These plots exhibit classic VRS characteristics, with very large, regular thrust oscillations. In order to verify the regularity of this process, the same parameters (α=60°, V=25 cm/s, θ=11.9°) were used for a 100 revolution run, followed by a 500 revolution run (see Fig. 8). Performance parameters and thrust time-histories for the two tests were nearly identical, validating the regularity of the process. The mean thrust coefficients for the two cases were 0.0137 and 0.0135, their peak-to-peak variations were 84 and 94% of the mean, and the average fluctuation periods were approximately 43 and 41 revolutions.

Other descent configurations demonstrated very similar oscillatory characteristics, but with significantly different amplitudes and periods of fluctuation. Figure 9 shows a thrust coefficient time-history that appears very similar to Fig. 8. However, in this case – where the descent angle was 50° and the descent speed was 30 cm/s – the

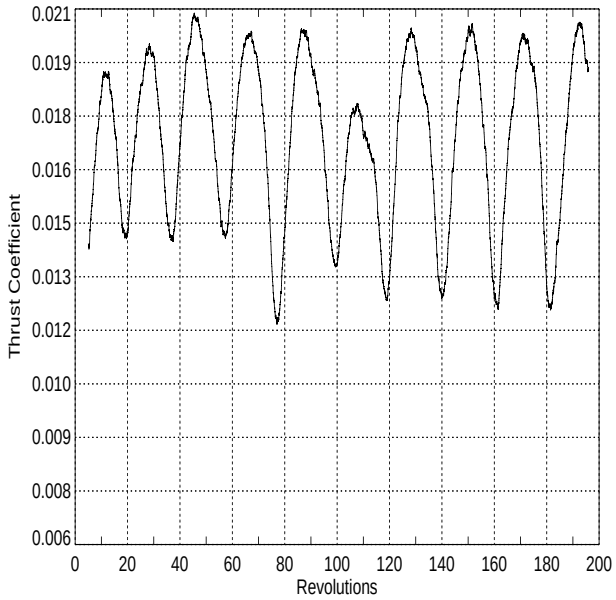

Fig. 9 Thrust time-history for another VRS case with α=50° and V=30 cm/s (μ=0.06). Mean thrust coefficient is 0.0173 and fluctuation is 50% of the mean. Fluctuation period in this case is only about 20 revolutions.

thrust oscillations were smaller in magnitude (peak-to-peak variation was 50% of the mean) and of shorter period (approximately 20 revolutions). The mean thrust coefficient in this case was slightly higher though, at 0.0173.

Obviously the descent configuration greatly influences the oscillatory behavior of the rotor thrust and thus can spell the difference between a routine bumpy ride and a catastrophic loss of control for a descending aircraft. This difference can be seen by comparing the thrust envelopes – the region between maximum and minimum thrust levels – for two descent angles over a range of descent speeds. Figure 10 shows the thrust envelopes for (a) α=90° and (b) α=60° descent configurations. For the vertical descent case (α=90°), the thrust levels dropped precipitously as the descent speed increased to about 20 cm/s. However, there was no noticeable thrust periodicity accompanying the loss of lift as one would see with a classic vortex ring state case. As the descent rate increased further, thrust was recovered and eventually reached two to three times hover thrust levels as the rotor encountered turbulent wake state and windmill brake state. The rotor's behavior in α=60° descent is similar, with loss of lift at approximately 20 cm/s, followed by recovery and increased lift as the descent speed reaches windmill brake state. The major difference between the two cases is in the size of the envelope. In vertical descent, the thrust levels drop drastically in the 20–40 cm/s descent speed range, yet the difference between maximum and minimum thrust levels is relatively small and also somewhat random. However, in the case of the α=60° descent, the rotor experiences not only a reduction in lift once VRS is reached, but also the large, regular oscillations in thrust as well. Thus the thrust envelope for this case is noticeably larger – covering a significant proportion of the total thrust. Controllability of the helicopter under these conditions is a major question.

Figure 11 provides a detailed look at the dynamics of the vortex ring formation and shedding process that precipitates the thrust oscillations discussed above. In (a), the rotor is relatively free of vorticity and the flow seems fairly orderly – hence the thrust is near its peak level. The incoming flow keeps the tip vortices near the rotor plane after they are generated and they begin to roll up into a thick ring in (b), interfering with the rotor's inflow and causing the thrust level to drop accordingly. In (c), a strong, tight ring can be seen to have formed at the back side of the rotor as the thrust approaches its minimum value. The ring begins to expand and separate from the back of the rotor slightly in (d) and (e), just as it starts to take form at the front of the rotor. This "halo" geometry, where the vortex ring is approximately equal in size and strength at the front and back side of the rotor, roughly coincides with the absolute minimum thrust level seen in the cycle. Finally, in (f), the ring has almost fully detached from the rotor plane and is quickly convected away upstream as the thrust level rebounds sharply.

This entire sequence of images – showing the complete formation, strengthening, and shedding process – spans only 11 revolutions, although the total peak-to-peak oscillation cycle takes about 36 revolutions. Given the metronomic regularity of the thrust time-history for this run, as well as those shown in Figs. 8–9, it seems clear that this process is highly deterministic and that the detachment of the vortex ring was not due to some flow disturbance or anomaly.

3.3 Summary Statistics

A primary interest of the rotorcraft community is the determination of the VRS boundary – the region of the flight envelope in which VRS conditions are likely to be encountered. Numerous methods have been employed for quantifying the magnitude of the thrust fluctuation levels and thus defining this boundary. Betzina [10] has proposed using three

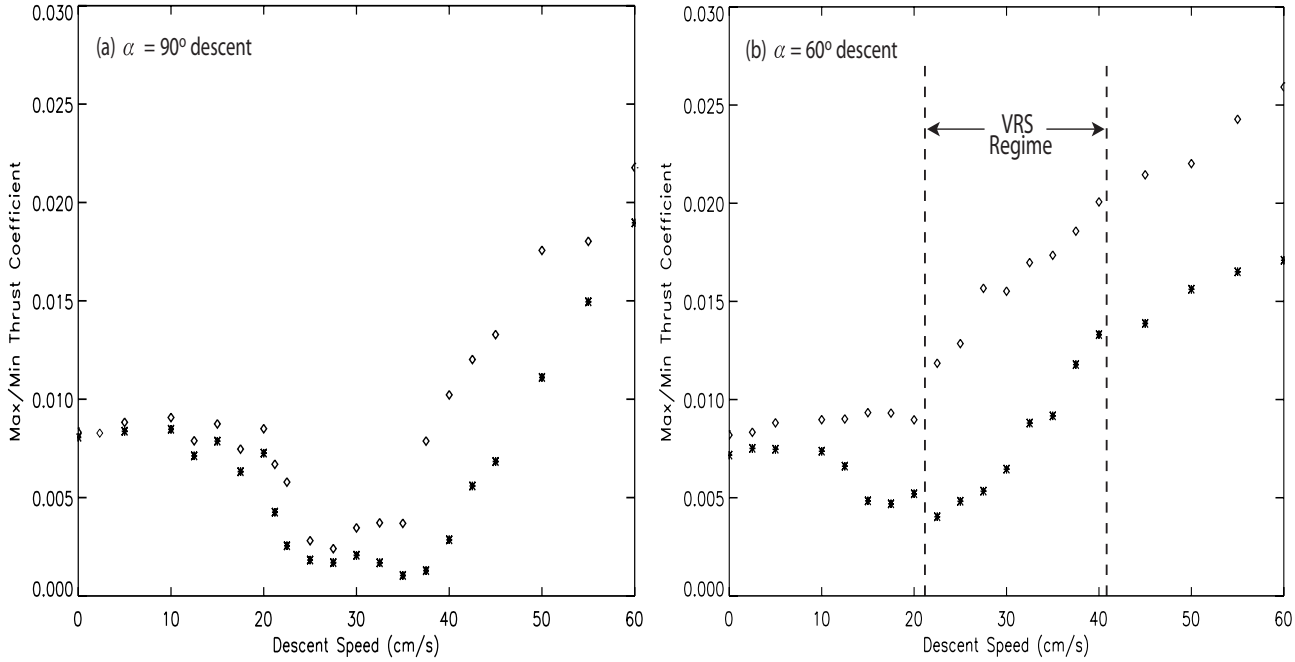

Fig. 10 Thrust coefficient envelopes – maximum and minimum thrust levels – for (a) 90° descent and (b) 60° descent configurations.

standard deviations of the thrust coefficient (3σ) normalized by the mean value. This measure is said to be more consistent than simply the peak-to-peak amplitude of the oscillations, and also less dependent on the length of the run and will thus be used in this study.

Figure 12 shows a contour plot of this parameter for all test runs, plotted with respect to advance and descent ratios, μ and ξ. Clearly the area featuring moderate forward and descent rates exhibits the most dramatic oscillations, as discussed earlier. It is difficult for anyone but an experienced helicopter pilot to specify how large the thrust fluctuations must be for the rotor to be considered in VRS. However, judging by the relative magnitude of the thrust fluctuations shown in Fig. 12, the region in the center of the plot – between about α=30° and 70° – is clearly set apart from the rest of the flight envelope.

Figure 13 shows the peak-to-peak amplitude of thrust fluctuations. Although not apparent from Fig. 12, it is clear that the amplitude of the thrust oscillations is still quite large in forward flight regimes. However, the mean rotor thrust in forward flight is significantly greater than in descent, thus the relative magnitude of the oscillations is less dramatic.

The behavior of the thrust fluctuations with respect to the forward flight speed is not quite as straightforward, as shown in Fig. 14. At large advance rates (μ>0.06) the wake is swept away behind the rotor, and so there is very little interaction between the rotor and its wake and thus little fluctuation in the thrust. However, at moderate advance rates the thrust fluctuations can be much more severe, depending on the rate of descent. This explains the wide scatter of the fluctuations seen in Fig. 14 for μ=0.02–0.05. Interestingly, at low advance rates (μ<0.01), the thrust fluctuations are again minimal, irrespective of the descent rate.

As discussed above, for the VRS cases, the oscillation frequencies and amplitudes varied significantly, depending on the descent configuration. The oscillation periods ranged anywhere from 20 to 50 revolutions, and the amplitudes of the fluctuations measured from 50% to 95% of the mean. Figure 15 shows the

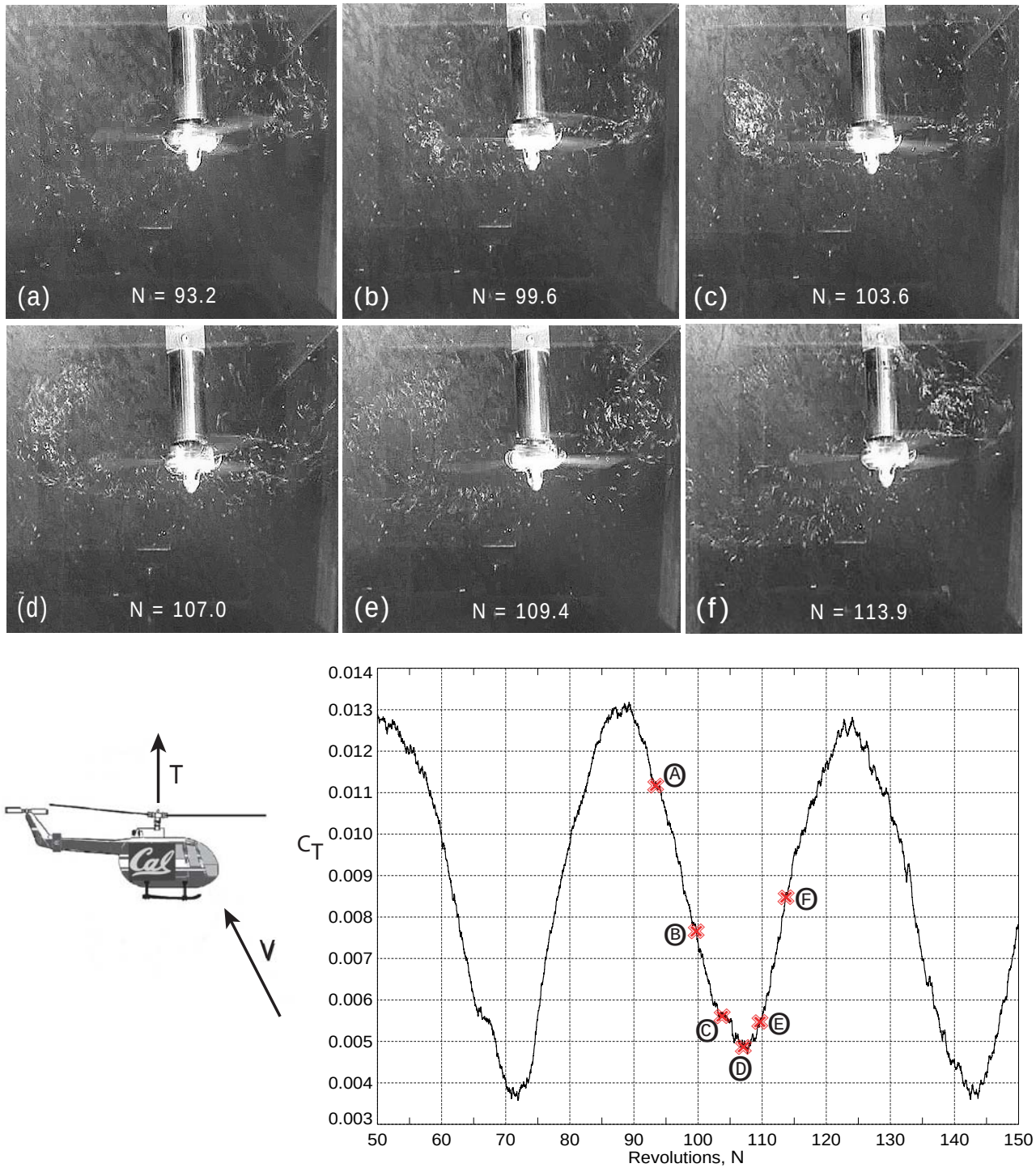

Fig. 11 Sequence of images depicting the various stages of vortex ring formation and shedding during VRS. Number of revolutions (N) since the beginning of the run is shown in each image for reference. Corresponding thrust coefficient time-history shows the resultant loss and recovery of lift during the cycle. Helicopter at lower left represents the rotor orientation and oncoming flow direction. Test parameters for this case were: α=60°, V=20 cm/s, Ω=3 rev/s, θ=11.9° (μ=0.042, ξ=-0.072). Mean thrust coefficient was 0.0086 and peak-to-peak variation was 121% of the mean, with a fluctuation period of 36 revolutions.

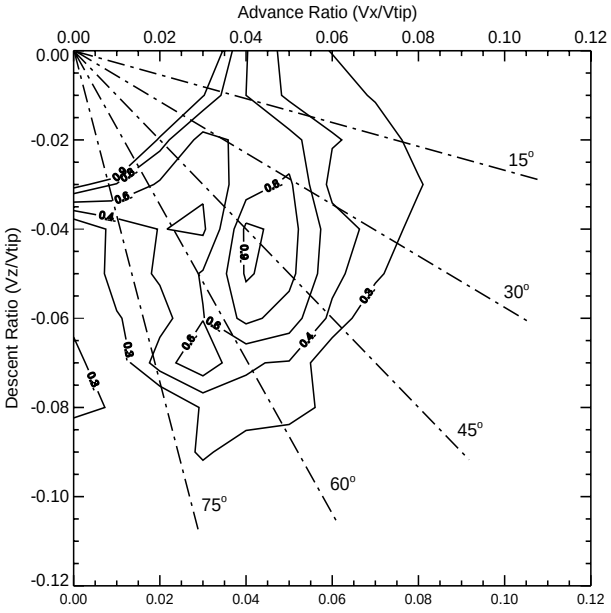

Fig. 12 Relative magnitude of thrust oscillations, $3\sigma/C_{T_{avg}}$ (θ=11.9° runs only).

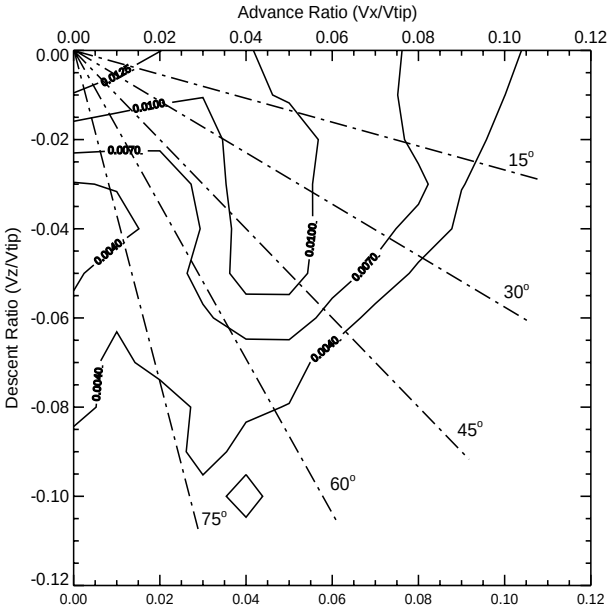

Fig. 13 Amplitude of peak-to-peak thrust coefficient oscillations, $C_{T_{max}} - C_{T_{min}}$ (θ=11.9° runs only).

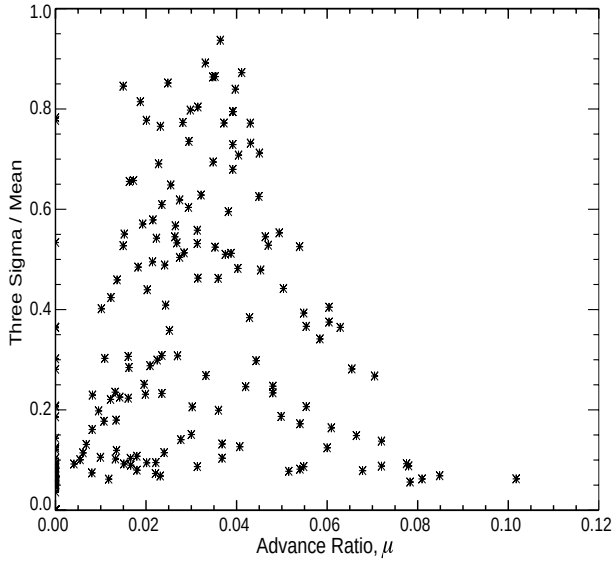

Fig. 14 Relative magnitude of thrust oscillations, $3\sigma/C_{T_{avg}}$, versus advance ratio, μ (θ=11.9° runs only).

relationship between the oscillation period and the advance ratio for the cases with observable, organized VRS-like oscillations. Data are plotted for a range of collective angle settings (from θ=6–17.5°), with a different power law regression for each setting. The trend shown here is not unusual – one would expect the vortex ring to be less stable and thus to be shed more rapidly as the advance rate increases. What is unusual is how well the power law relationships represent the data. The three regression equations, along with their correlation coefficients, are as follows:

θ=6.0°: $\tau = 0.33\ \mu^{-1.34}$ $R^2 = 0.96$
θ=9.0°: $\tau = 0.33\ \mu^{-1.41}$ $R^2 = 0.98$
θ=17.5°: $\tau = 0.18\ \mu^{-1.70}$ $R^2 = 0.79$

The relationship observed here between oscillation period and collective angle – that for a given advance ratio, the shedding period increases with collective angle – provides some clue as to the dynamics of the vortex ring shedding process. As the collective angle (and, therefore, the total lift) are increased, the strength of the tip vortices increases proportionally. In the vortex ring state regime, this equates to a stronger vortex ring with a greater self-induced velocity. This self-induction is ef-

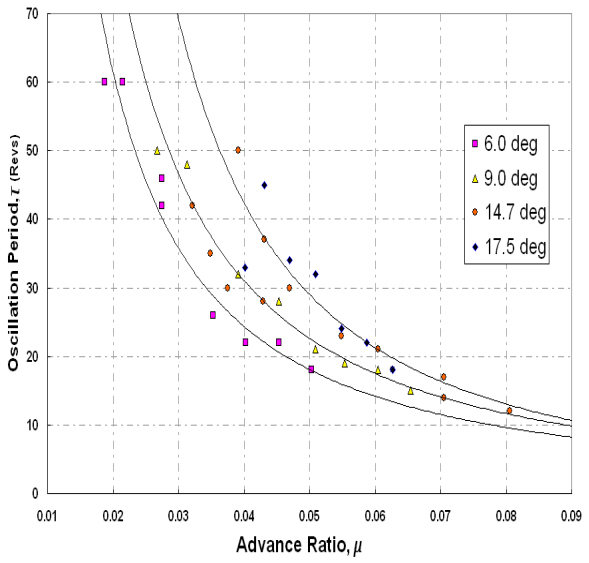

Fig. 15 Variation of the oscillation period, τ, with advance ratio, μ, for cases with observable VRS-like fluctuations. The data points shown are the "organized" fluctuations only. Collective angles range from θ=6–17.5°.

fectively the force holding the growing ring to the rotor plane and preventing it from convecting away with the free stream. Hence, with greater self-induced (downward) velocity comes longer attachment periods between the ring and the rotor plane.

4 Concluding Remarks

Flow visualization and thrust measurement experiments have been performed on a three-bladed rotor model in two water tanks. Descent angle and speed have been varied in order to simulate a wide range of descent configurations, with particular emphasis on the vortex ring state regime. Some of the specific conclusions from this study are:

1. Flow visualization images from the hovering rotor capture both the short- and long-wave instabilities that develop in the near-wake of the rotor and precipitate its rapid breakdown. The location where the wake breaks down and loses its structure can be seen to be approximately one diameter downstream of the rotor.

2. Flow visualization images from the descending rotor operating in the VRS regime show the merger of the individual tip vortices and the formation of a thick vortex ring. This ring would remain just above the rotor plane for a period of 20–50 revolutions (depending on advance ratio, descent ratio, and tip speed) before abruptly detaching and convecting away upstream while another ring would begin to form.

3. Correlations between flow visualization images and instantaneous thrust measurements indicate a severe reduction in rotor thrust when the vortex ring is "attached" to the rotor, followed by a full recovery of thrust once it is shed.

4. The regularity of the vortex ring shedding/formation process over 100–500 revolution periods indicates that the process is quite stable and is likely dictated by the size of the ring and the amount of vorticity it can contain.

5. Thrust fluctuations observed in the VRS regime were most severe for descent angles of α=20–50° and for descent speeds of V=20–30 cm/s. In this region, the peak-to-peak amplitudes of the thrust fluctuations were approximately 80–95% of the mean thrust. Thrust oscillations of this magnitude will have a potentially disastrous effect on the performance and control of a helicopter or a tiltrotor aircraft and are thus deserving of further study.

6. In VRS cases, the vortex ring shedding period exhibits a decaying power law dependence on the advance ratio, indicating that the ring is less stable and more susceptible to being swept away from the

rotor as advance speed increases. Additionally, the shedding period appears to increase slightly with collective angle.

7. To gain a more complete understanding of the flow physics in this flight regime it will be necessary to perform PIV experiments on the critical descent configurations identified in this paper. By collecting quantitative information about the flow field in the VRS regime it should be possible to better understand the nature of the highly regular vortex ring shedding/formation process was observed here. And with knowledge of the dynamics of VRS, it should eventually be possible to mitigate or avoid the severe thrust fluctuations associated with it.

References

[1] Levy, H., and Forsdyke, A. G., "The Steady Motion and Stability of a Helical Vortex," *Proceedings of the Royal Society of London. Series A*, Vol. 120, (786), 1928, pp. 670-690.

[2] Landgrebe, A. J., "An Analytical Method for Predicting Rotor Wake Geometry," *Journal of the American Helicopter Society*, Vol. 14, (4), 1969, pp. 20-32.

[3] Widnall, S. E., "The Stability of a Helical Vortex Filament," *Journal of Fluid Mechanics*, Vol. 54, Pt. 4, 1972, pp. 641-663.

[4] Gupta, B. P., and Loewy, R. G., "Theoretical Analysis of the Hydrodynamic Stability of Multiple Interdigitated Helical Vortices," *AIAA Journal*, Vol. 12, (10), 1974, pp. 1381-1387.

[5] Stanchfield, M., "Flight Dynamics: Vortex Ring State Revisited," *Aviation Today*, November 2001.

[6] Glauert, H., "The Analysis of Experimental Results in the Windmill Brake and Vortex Ring States of an Airscrew," Rept. 1026, Aeronautical Research Committee, 1926.

[7] Drees, J. M., and Hendal, W. P., "The Field of Flow through a Helicopter Rotor Obtained from Wind Tunnel Smoke Tests," *Journal of Aircraft Engineering*, Vol. 23, (266), 1951, pp. 107-111.

[8] Washizu, K., Azuma, A., Koo, J., and Oka, T., "Experiments on a Model Helicopter Rotor Operating in the Vortex Ring State," *Journal of Aircraft*, Vol. 3, (3), May-June 1966, pp. 225-230.

[9] Abrego, A., and Long, K., "A Wind Tunnel Investigation of a Small-scale Tiltrotor in Descending Flight," Proceedings of the American Helicopter Society Aerodynamics, Acoustics, and Test and Evaluation Meeting, San Francisco, CA, January 2002.

[10] Betzina, M., "Tiltrotor Descent Aerodynamics: Small-Scale Experimental Investigation of Vortex Ring State," 57th Annual Forum of the American Helicopter Society, Washington, DC, May 2001.

[11] Fukumoto, Y., and Miyazaki, T., "Three-dimensional Distortions of a Vortex Filament with Axial Velocity," *Journal of Fluid Mechanics*, Vol. 222, January 1991, pp. 369-416.

[12] Ortega, J. M., Caradonna, F., Savaş, Ö, "An Experimental Study of the Stability of Helical Vortices in a Propeller Wake," submitted for publication in *Journal of Fluid Mechanics*, 2003.

[13] Jain, R., and Conlisk, A. T., "Interaction of Tip-Vortices in the Wake of a Two-Bladed Rotor in Axial Flight," *Journal of the American Helicopter Society*, Vol. 45, (3), July 2000, pp. 157-164.